TECHNICAL RESEARCH REPORT

SYSTEMS RESEARCH CENTER

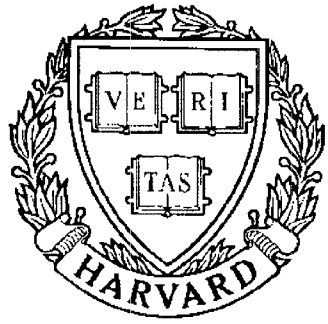

Supported by the National Science Foundation Engineering Research Center Program (NSFD CD 8803012), Industry and the University

On the Dynamics and Global Stability Characteristics of Adaptive Systems

by R.A. Adomaitis, C.E. Frouzakis and I.G. Kevrekidis

TR 91-100

On the Dynamics and Global Stability Characteristics of Adaptive Systems

Raymond A. Adomaitis
Systems Research Center
University of Maryland
College Park, MD 20742

Christos E. Frouzakis and Ioannis G. Kevrekidis
Department of Chemical Engineering
Princeton University
Princeton, NJ 08544

Manuscript date: November 1991.

Abstract

We consider the dynamics of some representative adaptively-controlled systems and focus on situations where the desired operating point is locally, but not globally, stable. Perturbations which drive the system from the set point are quantified by computing the boundaries separating the basin of attraction of the set point from the basins of attraction of the other, undesirable attractors. The basins are found to sometimes consist of complicated, disconnected structures in phase space. This results from the nonunique reverse-time dynamics often exhibited by these systems and can be studied by considering the behavior of the reverse-time map along the basin boundaries. The effect of noninvertibility on the forward-time dynamical behavior is also explored.

Introduction

Adaptive control schemes can be used when the form of a model describing the open-loop dynamics of the plant is known but some or all of the parameters are unknown or vary slowly in time. Global stability of the desired operating point can be assured in some cases of no plant/reference-model mismatch (e.g., Goodwin *et. al.*, 1980), but complicated dynamics can result in cases of sufficient mismatch (Golden and Ydstie, 1988; Mareels and Bitmead, 1986, 1988; Frouzakis *et. al.*, 1991). One type of behavior we will discuss in detail is *multistability*: situations where the locally-stable set point coexists with another, undesirable attractor. In cases of multistability, it becomes important to know which perturbations drive the controlled system from the desired operating point. The set of perturbations from which the system returns to the desired operating point constitutes the *basin of attraction* of the set point. Methods for computing the boundaries separating different basins of attraction will be used rather than the brute-force method of approximating the entire basin region.

Analysis of the global dynamical features of the systems to be discussed proceeds in two steps: 1) the fixed points, periodic points, and other equilibrium solutions are found and their local stability is determined; 2) approximations of the local stable manifolds of the saddle-type periodic points[1] are made and then followed backward in time. It is the second step which gives the basin boundaries. In some cases, we find that the boundaries exhibit unusual, disconnected and distorted shapes. This results from the *noninvertible* nature of these discrete-time systems. The mappings discussed all have uniquely-determined forward-time trajectories, but may have branching trajectories in reverse-time with the

[1] The local saddle-stable manifold W^s_{loc} is defined by all the points in the neighborhood of the saddle point which asymptotically approach the saddle in forward time.

branching behavior being a function of phase-space location. This behavior is fundamentally different from that displayed by invertible systems, systems which have a unique *preimage* (the set of initial conditions that give a particular point) for every point in phase space. We will see that the complicated basin structures sometimes found for noninvertible systems are due to the exponential growth of preimages of a basin region followed in reverse-time.

A Representative Adaptive System

Consider controlling the open-loop plant:

$$y_{n+1} = ay_n + bu_n \tag{1}$$

where y is the state and u is the manipulated variable when the eigenvalue a is known approximately and b is unknown. The control action that would achieve dead-beat control if the system could be modeled exactly is derived by inverting a model which has the same form as (1) but with α as the estimate of a. Using an on-line estimator to determine the value of b (see Adomaitis and Kevrekidis, 1991), we find that the dynamics of the controlled system are described by:

$F : R^2 \mapsto R^2$

$$\begin{aligned} y_{n+1} &= ay_n + z_n, \\ z_{n+1} &= z_n \left[1 + \frac{(y_{n+1} - \alpha y_n)(\alpha y_n + 1 - y_{n+1} - \alpha y_{n+1})}{c + (y_{n+1} - \alpha y_n)^2} \right] \end{aligned} \tag{2}$$

where $z = bu$, the set point is $y = 1$, and c is a small, positive constant introduced to prevent division by zero in the control law. With no mismatch ($\alpha = a$), all initial conditions save $z = 0$ are mapped to the desired operating point ($y = 1, z = 1 - a$) in two iterations. To assess the effects of mismatch, we will fix $c = 0.005$ and $a = 0.5$, and vary α; the difference between α and a is the plant/model mismatch. A portion of the bifurcation behavior is presented in Fig. 1. We see that the set-point attractor is destabilized by a subcritical period-doubling bifurcation at $\alpha = 0.635$ that gives rise to a branch of saddle-type period-2 solutions. This branch collides with a branch of stable period-2 solutions during a saddle-node bifurcation at $\alpha = 0.616$; the stable period-2 branch then undergoes a series of period double bifurcations (the first takes place at $\alpha = 0.622$) and ultimately we find a complicated, possibly chaotic attractor. A similar bifurcation scenario is found when α is fixed at 0.621 and c is allowed to vary, except that the complicated attractor resulting from the period-doubling cascade is destroyed as

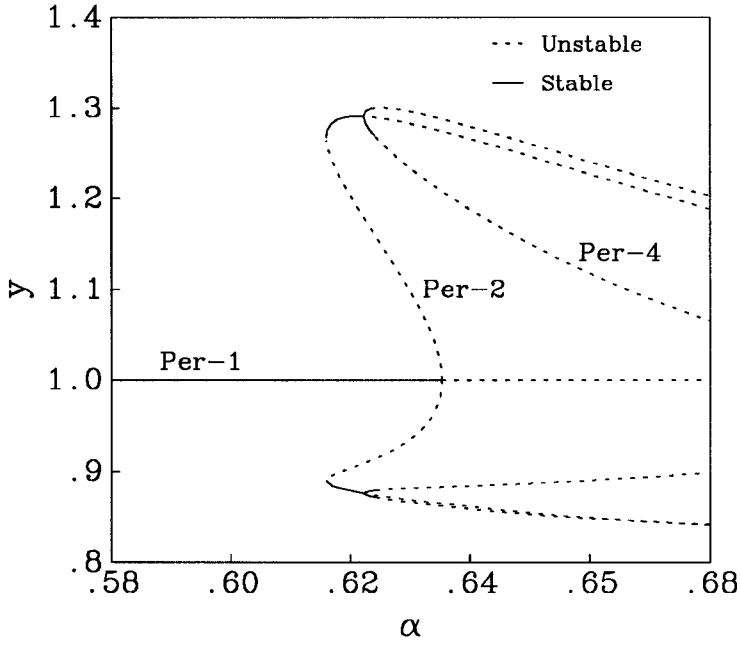

Figure 1 The bifurcation diagram of the map F illustrating the fixed and periodic solutions found as a function of mismatch $(\alpha - a)$ when $a = 0.5$ and $c = 0.005$.

a consequence of a homoclinic bifurcation at approximately $c = 0.00424$. More will be said on the implications of this global bifurcation in the next section.

We now see that there exists a range of plant/reference-model mismatch ($\alpha \in [0.616, 0.635]$) where a stable periodic attractor coexists with the locally-stable set point. This range lies between the saddle-node bifurcation of period-2 solutions and the period-1 period-doubling point of Fig. 1. Choosing a representative value of α in the range of multistability, the location of the fixed and periodic points can be plotted along with a portion of the preimages of the local saddle-stable manifold (W^s_{loc}) to find the boundaries separating the basin of attraction of the undesirable attractor from the desired operating point. When this is done with the F map (see Fig. 2 for $\alpha = 0.621$), we find that the basin of attraction of the period-2 solution is the union of an infinite number of disconnected and distorted patches of phase space. The disconnectedness is apparent in the shaded "island" that surrounds the lower stable period-2 point and the distortion is a reference to the way some of the shaded regions are pulled to positive and negative infinity. It should be noted that the level of complexity (there are an infinite number of disconnected shaded regions) of the period-2 basin structure cannot be discerned at the resolution level of Fig. 2.

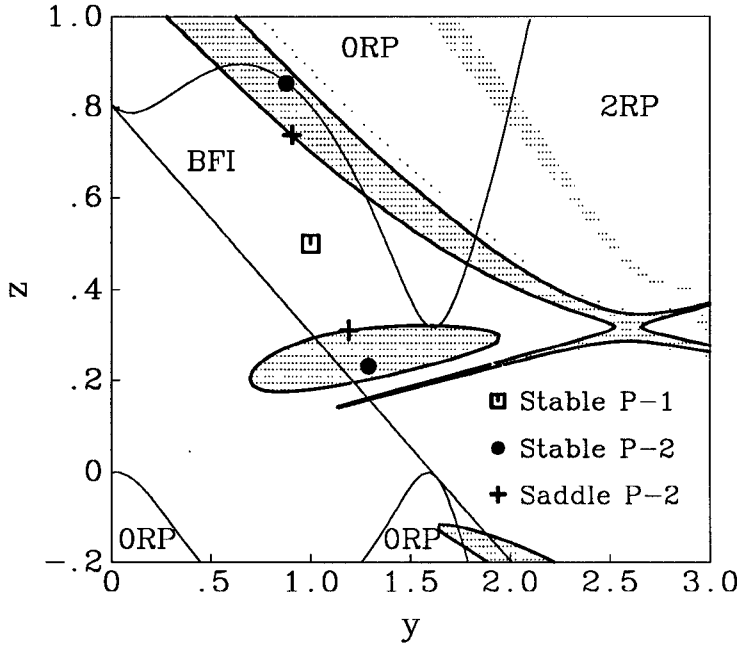

Figure 2 The basin of attraction of the period-2 point is shown as the shaded region. A portion of the *stablemanifold* of the saddle period-2 is also shown along with the preimage equation bifurcation loci. Parameter values are $\alpha = 0.621$, $c = 0.005$, and $a = 0.5$.

Before proceeding, we note that the origin is also a fixed point of F. It is marginally stable (the eigenvalues are 1 and a) and its local stable manifold is the line $z = 0$. For the parameter ranges considered in this work, the basin of attraction of this point was found to lie mostly outside the phase-space region shown in Fig. 2. This attractor will not be discussed further in this paper.

The reason for the complicated basin structure of Fig. 2 can be understood by first inverting the map describing the forward-time dynamics; we obtain a quadratic equation with coefficients that depend on the present location of the point (y_{n+1}, z_{n+1}). The reverse-time map consists of the solution of

$$\phi_1(y_{n+1}, z_{n+1})y_n^2 + \phi_2(y_{n+1}, z_{n+1})y_n + \phi_3(y_{n+1}, z_{n+1}) = 0 \qquad (3a)$$

where

$$\begin{aligned}
\phi_1(y_{n+1}, z_{n+1}) &= \alpha^2 z_{n+1} - a\alpha + a\alpha^2 y_{n+1}, \\
\phi_2(y_{n+1}, z_{n+1}) &= -2\alpha y_{n+1} z_{n+1} + \alpha y_{n+1} - \alpha^2 y_{n+1}^2 + ac + a y_{n+1} - a\alpha y_{n+1}^2, \\
\phi_3(y_{n+1}, z_{n+1}) &= c z_{n+1} + y_{n+1}^2 z_{n+1} - c y_{n+1} - y_{n+1}^2 + \alpha y_{n+1}^3
\end{aligned} \qquad (3b)$$

for y_n and the subsequent evaluation of

$$z_n = y_{n+1} - a y_n \qquad (4)$$

for z_n. This means there will be 0 to 2 preimages of every phase-space point, the number being 0 or 2 over regions of phase space separated by *turning-point bifurcations* of the roots of the reverse-time map (TPB curves occur when $\phi_2^2 - 4\phi_1\phi_3 = 0$). The phase space is also crossed by BFI (*bifurcations from infinity*) loci. These curves mark points in phase space which give one bounded root for (3) and one unbounded root (a preimage at infinity). As discussed in detail in Adomaitis and Kevrekidis (1991), the disconnected basin portions are due to basin regions crossing the TPB loci and the stretching to infinity is due to crossing the BFI curves.

The TPB curves are defined by the points in phase space which give a double real root of the reverse-time map. In the quadratic-inverse system discussed, the TPB curves will then possess a unique preimage. These period-1 preimages correspond points in phase space where the determinant of the Jacobian matrix of the *forward-time* map (F) vanishes. Gumowski and Mira (1980) call this curve J_0, its nth-period image J_n, and its nth-period preimage J_{-n}, e.g., the TPB curve is J_1. J_0 and all of its images and preimages define the set of *critical curves*. We will use this notation during the remainder of this paper.

While it has been established that the boundary of the basin of attraction of the period-2 point (and attractors resulting from period-doubling bifurcations of this point at other parameter values) is determined by the points in phase space which asymptotically approach the period-2 saddle points, we see that these points do not lie on a manifold because they do not form a continuous curve. We will refer to these structures as "stablemanifolds," the single-word term coined by R. P. McGehee to distinguish them from the invariant stable manifolds of invertible systems. We also note that while the boundaries separating different basins of attraction have been discussed, a means of differentiating points "inside" from those "outside" a particular stablemanifold segment is not immediately apparent. A brute-force method is to pick a single point inside each closed region and follow it forward in time, shading the regions corresponding to the period-2 solution basin of attraction.

Changes in Complexity Levels

In the previous Section, we saw that the inverse map of F was a function of both phase space location and the fixed system parameters. This means the shape and location of the critical curves will change with the parameters values. This can lead to qualitative changes in basin structure as system parameters are varied. A dramatic example of the different basin structures found for other parameter values is displayed in Fig. 4, where two holes are found in the basin of attraction

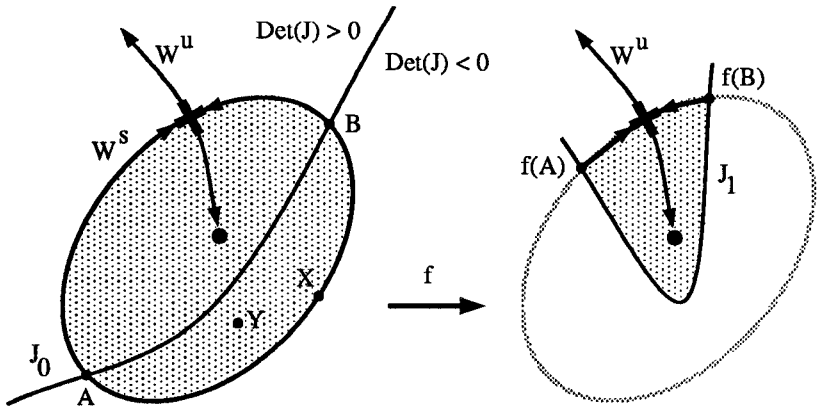

Figure 3 The image of the shaded region under f ($f = F \circ F$). J is the Jacobian matrix of f. We see that the saddle point (+) and the additional preimage X map to the saddle, and the fixed point (•) and Y map to the fixed point. Sets of points for which the determinant of J is positive preserve their orientation under f.

"island" surrounding the lower half of a stable higher-period point (this attractor results from a sequence of period-doubling bifurcations of the stable period-2 point of Fig. 2; the basin boundary still consists of the stablemanifold of the period-2 saddle point). These holes allow points to escape from the island-shaped region. This island is qualitatively different from the analogous period-2 basin region of Fig. 2 since *all* points inside the latter remain in the period-2 basin of attraction. The finite number of holes is observed to develop into an infinite number (and the undesirable attractor appears to have been destroyed) for $c \leq 0.00424$.

The means by which holes develop can be explained by first considering the hole-free case of the lower island basin portion of Fig. 2. A schematic of the island is shown in Fig. 3; it is important to note that the critical curves correspond to those of the period-2 map f (F^2) in this diagram. This simplifies the following discussion since references to the "upper" period-2 features are avoided. The attractor of Fig. 3 is marked by the larger • and the shaded region is its basin of attraction. The stablemanifold is denoted as W^s and the unstable manifold[2] by W^u. The closed outer boundary of the island is formed by preimages (f^{-1}) of the W^S segment immediately adjacent to the saddle point, extending in each direction to $f(A)$ and $f(B)$. Because these two points lie on J_1, their unique preimages lie on J_0 (points A and B of the left-hand-side of Fig. 3). The portion of W^s in between $f(A)$ and $f(B)$ has two real preimages[3] that join smoothly

[2] The points in phase space which asymptotically approach the saddle point in reverse time. A more extensive discussion of the behaviors exhibited by W^u is found in the "Forward-Time Dynamics" section of this paper.

[3] Strictly speaking, the upper portion of W^s 4 preimages. However, one of the first 2 preimages is premapped outside this local region of phase space and so plays no role in the basin boundary structures discussed. The other is premapped up to the upper period-2 saddle point and has the two preimages relevant to this analysis.

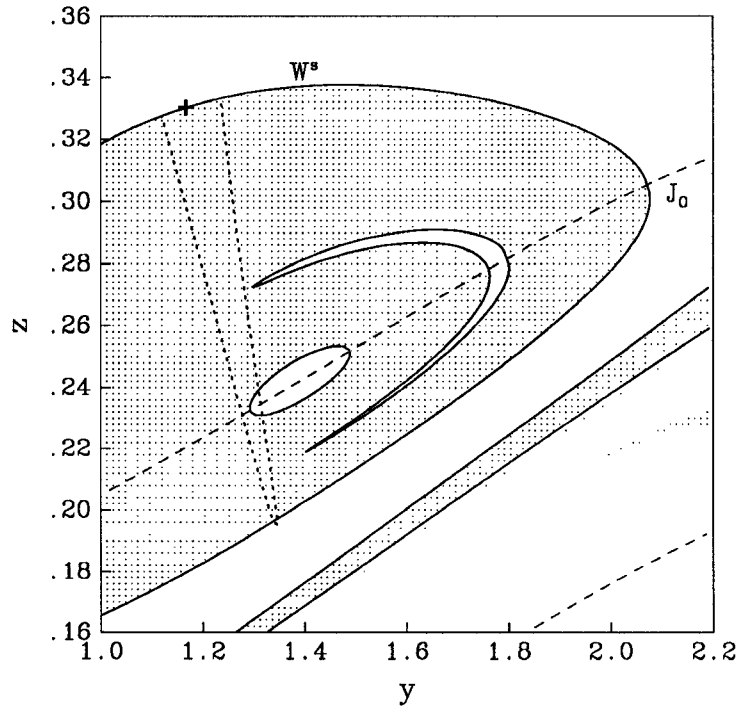

Figure 4 Holes inside the "island" portion of the basin of attraction of the undesirable attractor. The high-period, undersirable attractor is not shown, but it lies inside the island. The holes are the smaller white regions inside the shaded region. The image of the portion of J_0 inside the island is the short-dash, wedge-shaped curve. Parameter values are $\alpha = 0.621$, $c = 0.00425$, and $a = 0.5$.

at the gluing points A and B. This means the island structure is composed of two regions, each of which is mapped to the wedge-shaped shaded region of the right-hand-figure of Fig. 3. We call the region inside W^s the "apparent" basin of attraction of the period-2 point since, with no other information, one might conclude that all points in the region up to W^s surrounding the attractor are in its basin of attraction. This conclusion is valid in the case of Fig. 3 since the image of the island lies completely within the island, and so no points can escape from the apparent basin of attraction. This is not always the case, however, and Fig. 4 (and the enlarged view in Fig. 5) shows an example. We see that the tip of wedge-shaped image of the island extends just beyond W^s. This means that the portion of phase space inside the wedge but outside the island (see Fig. 5) has two preimages inside the island. Both preimages glue smoothly at J_0 (since the outer boundary of the wedge is J_1). The points inside this hole leave the island in one iteration of f and never return—this is how points in the "apparent" basin of attraction escape.

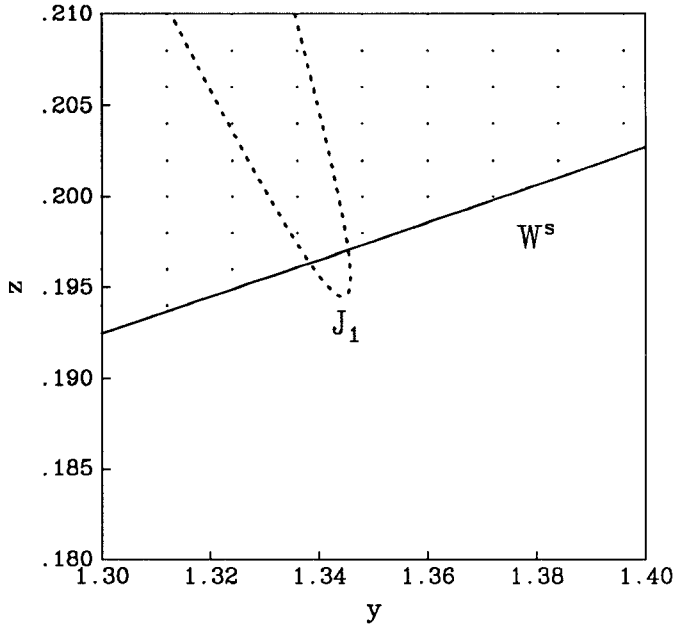

Figure 5 A more detailed look at the previous Figure showing the image of J_0 (labeled J_1) does indeed fall partially outside the "apparent" basin boundary (defined by W^s).

This explains the first (and smaller) hole. In this case of two holes, the first hole lies partly inside the wedge-shaped image of the apparent basin of attraction. The portion of the first hole lying inside the wedge will also have two preimages within the apparent basin that connect at J_0, forming the second hole. The second hole lies completely outside of the wedge and so has no preimages inside the island. Thus, we find a finite number of holes (finite complexity) for this set of parameter values. However, when a segment of W^u is plotted for the case of $c = 0.00424$, (see Fig. 6) we see that it intersects the first hole, allowing it to have at least one infinitely-preiterable path (in reverse-time), and so an infinite number of holes results. This is, in fact, a homoclinic bifurcation and we observe that the attractor is destroyed as a consequence of this global bifurcation. The onset of infinite complexity for a map which actually gives a computable criterion marking this transition has been been discussed in detail in Adomaitis *et. al.* (1991).

A Cubic-Root System

In the F map, it was assumed we had a good estimate of the open-loop eigenvalue and on-line estimation of the gain of the manipulated variable b was performed. In the case of on-line estimation of a and a fixed estimate of b, we obtain the G map (Golden and Ydstie, 1988; Adomaitis and Kevrekidis, 1990):

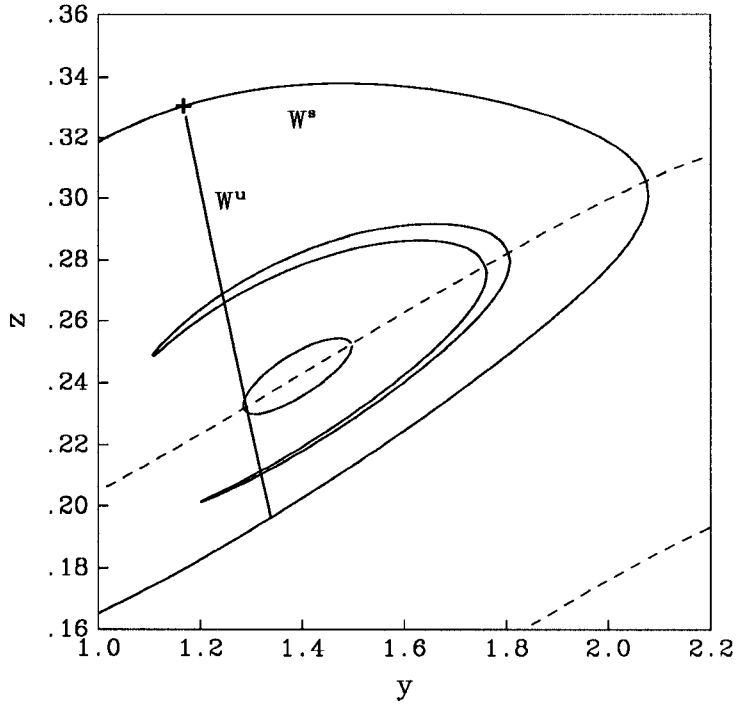

Figure 6 Infinite basin complexity displayed by the F map for $\alpha = 0.621$, $c = 0.00424$, and $a = 0.5$. Only the first two of an infinite number of hole boundaries are shown.

$G : R^2 \mapsto R^2$

$$\begin{aligned} y_{n+1} &= z_n y_n + k, \\ z_{n+1} &= z_n - \frac{k y_n}{c + y_n^2}(z_n y_n + k - 1) \end{aligned} \tag{5}$$

where k is the ratio of the actual value of b to its assumed value and c again prevents division by zero. In addition to a subcritical period-doubling bifurcation of the set-point branch (as in the F map), the G map also exhibits isolated periodic solution branches (see Fig. 7). This map differs fundamentally from F with respect to its preimage behavior in that G has from 1 to 3 preimages (as opposed to the 0 to 2 preimages of F). The inverse map G^{-1} is found by the solution of

$$c z_n^3 - c z_{n+1} z_n^2 + y_{n+1}(y_{n+1} - k)(1 - k) z_n - z_{n+1}(y_{n+1} - k)^2 = 0 \tag{6}$$

for z_n with subsequent evaluation of

$$y_n = \frac{y_{n+1} - k}{z_n} \tag{7}$$

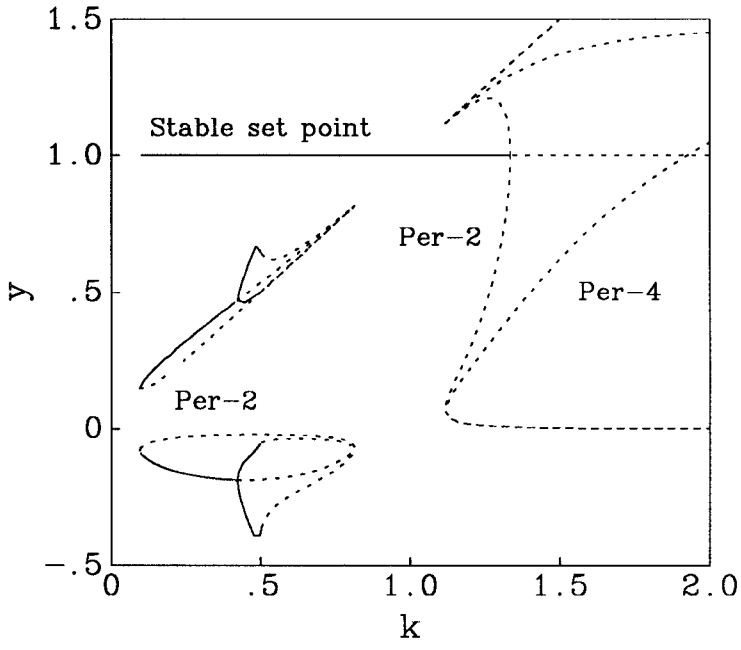

Figure 7 A portion of the G map bifurcation diagram for $c = 0.005$. Dashed curves indicate branches of unstable solutions.

for y_n. This system has regions of phase space whose points have a unique preimage and regions of points with three real preimages. This can give rise to "normal-looking" basin boundaries when W^s does not interact with the 3-real-preimage (3RP) region.

Another situation that leads to "normal-looking" basin boundaries is depicted in Fig. 8, a schematic illustrating end-to-end gluing of stablemanifold segments. In this diagram, we see a period-2 saddle point (marked by the + symbols) and segments of its W^s. The right-hand saddle point (point c) lies inside the 3RP region as does its W^s_{loc}. This means the saddle point and W^s_{loc} (up to the points "a" and "b") have three preimages. One of the preimages of the saddle "c" is the other period-2 saddle point and the other two mark *points of alternance* (in the terminology of Gumowski and Mira, 1980). Because W^s enters through different sides of the 3RP region, the gluing of W^s segments gives one curve and does not result in islands, as would be the case if both sides of W^s entered through the same 3RP boundary (similar roots appear/disappear on similar "sides" of the 3RP region; the boundaries of the sides are the cusps). So we see that while the direction of evolution changes along the stablemanifold at the points of alternance, the overall boundary remains smooth and continuous. The break up into a fishbone-shaped basin of attraction is caused by the saddle-stablemanifold

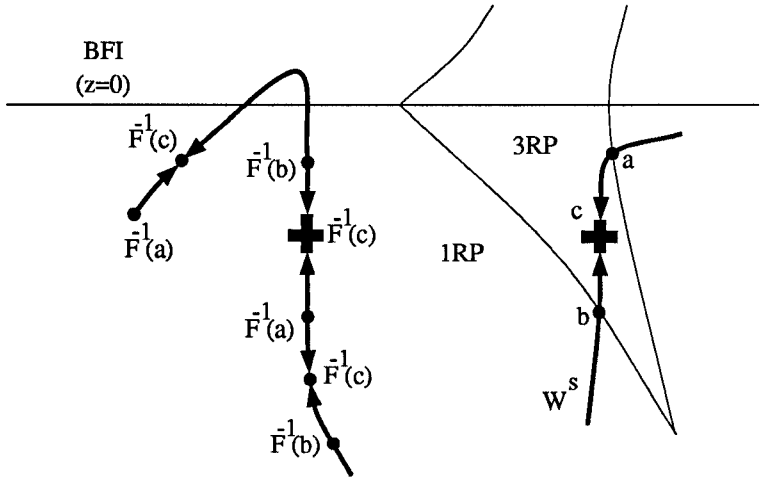

Figure 8 End-to-end gluing and the distortion due to a preimage BFI curve at $z = 0$.

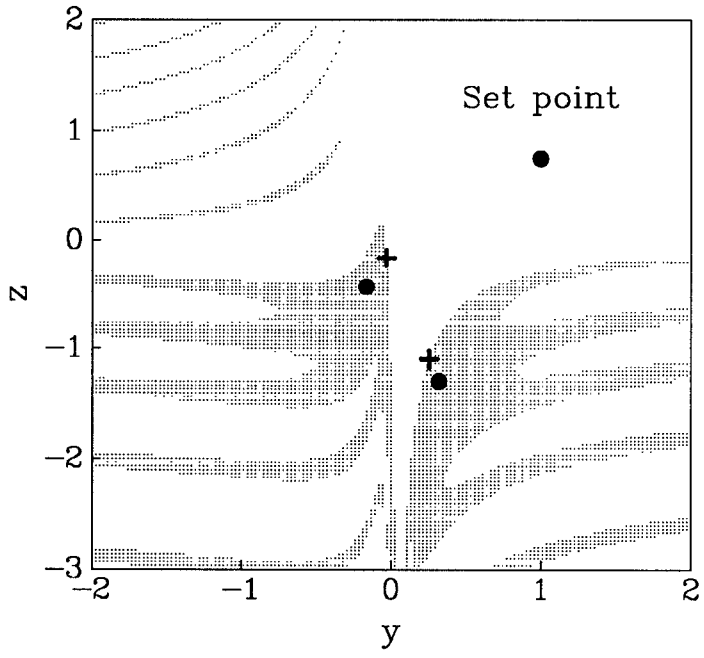

Figure 9 The basin of attraction of the period-2 point is shown as the shaded region. Parameter values are $k = 0.25$ and $c = 0.005$.

crossing the BFI line defined by $z = 0$. It is easy to show that preimages of points in the region ($y < 0$, $z > 0$) remain there and so the disconnected patches of period-2 basin of attraction in this region are all preimages of the small hump of the "main" portion of the basin of attraction that extends above $z = 0$ (Fig. 9).

Forward-Time Dynamics

As we saw in the discussion of complexity, phase space folding in forward-time is associated with changes in the number of preimages as a function of phase-space location. This means if a portion of a local saddle-unstable manifold (W^u_{loc}) is computed and then followed forward in time to find W^u, images of W^u_{loc} may fold in such a way as to form kinks, loops, and more complicated structures. While the images will always lie on a continuous curve, we will refer to it as the *unstablemanifold* when it is not differentiable or self-intersects. If a portion of W^u falls into a region where the map has more than one preimage, that segment of W^u will have preimages which do not asymptotically approach the saddle point in reverse-time. With this in mind, consider the dynamics of an adaptively-controlled system where there is additional mismatch due to an unmodeled, constant disturbance (Frouzakis, 1991):

$H : R^2 \mapsto R^2$

$$\begin{aligned} y_{n+1} &= -y_n z_n + v, \\ z_{n+1} &= -z_n + \frac{p y_n}{c + y_n^2}(-z_n y_n + v - 1). \end{aligned} \tag{8}$$

The constant v is composed of k (c.f. the G map) and the unmodeled disturbance, and p is a function of k and an indentifier gain. Notice how the form of H is basically the same as G and so we expect 3RP and 1RP regions.

We illustrate several different forward-time behaviors exhibited by this system with a sequence of phase portraits, beginning with a period-30 attractor coexisting with a period-30 saddle point shown in Fig. 10. The series of bifurcations that takes place after the set point (not shown in Fig. 10) becomes unstable and gives rise to this phase portrait is discussed in Frouzakis (1991). A closer look at one of the saddle points is shown in Fig. 11 along with the saddle-unstable manifold segments we calculate, each side asymptotically approaching a stable period-30 point. Because the periodic points and the saddle-unstable manifolds all lie completely within the 1RP region, the behavior is the same as what is displayed by diffeomorphisms (hence the use of the two-word term "unstable manifold"). However, as we increase the magnitude of the unmodeled error (decreasing the negative v), we see that a portion of W^u dips into the 3RP region (Fig. 12). This segment (denoted Γ) has one preimage on the main part of W^u and since it enters and leaves through the *same* boundary of the 3RP region, it has two additional preimages that glue to each other. The first is the closed curve $H^{-1}(\Gamma)$ of Fig. 13. This curve lies in the 1RP region and has an infinite number of preimages ($H^{-2}(\Gamma)$ and so on) that asymptotically approach the set point in reverse-time.

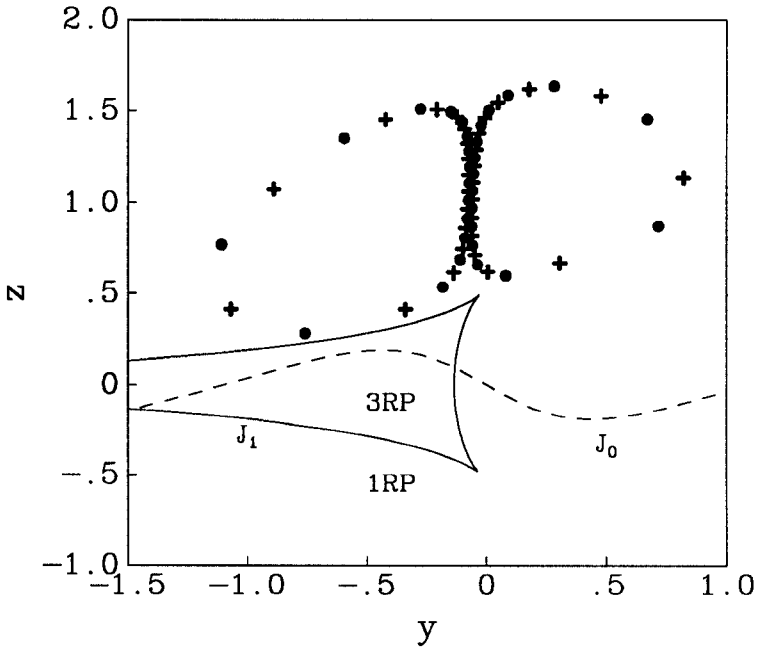

Figure 10 The H map for $v = -0.135$, $p = 0.8$, and $c = 1.2$. The $+$ symbols denote the period-30 saddle point and the $\bullet$ symbols the period-30 node.

As we continue to increase the magnitude of the unmodeled error, we observe W^u change from a diffeomorphism-like unstable manifold to the more complicated, self-intersecting curve shown in Fig. 14 (recall that it is the images of W^u_{loc} being discussed and not the excess preimages of portions of W^u). This is a consequence of the unstablemanifold crossing J_0, and the sequence of transitions which ultimately gives this behavior is shown in Fig. 15. Several of the behaviors have been observed previously (see Fig. 13 of Lorenz, 1989).

The image of a curve segment passing through J_0 generically will be another curve tangent to J_1 at the image of the two intersection points. The segment image will not cross J_1 in the neighborhood of the intersection images, but instead will bend away in a quadratic manner. In Fig. 15A, we see that when W^u first crosses J_0, the image of this segment of W^u will tangentially touch J_1 twice. The two intersections of W^u and J_1 are unrelated to the interactions of the preimage of the W^u segment and J_0, unless W^u passes through the cusp (see Fig. 15B). After passing though the cusp, the preimage of the cusp on J_0 lies between the two intersections of W^u and J_0 (see Fig. 15C). Note that the transitions to this point have done nothing to change the status of W^u from a manifold.

The transition to an unstablemanifold is depicted in Fig. 15D. For this value of v, the left intersection of W^u and J^0 occurs such that W^u is tangent to

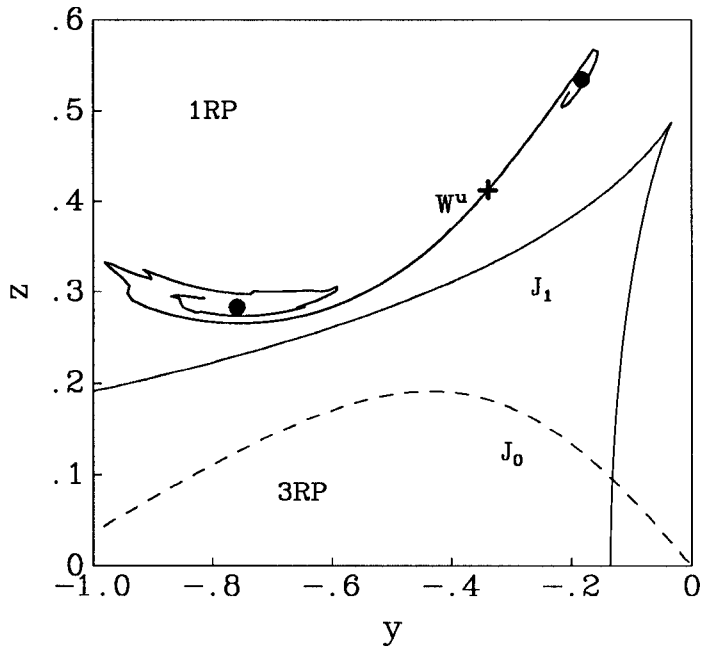

Figure 11 A closer look at the previous Figure showing the saddle-unstable manifolds completely outside the 3RP region.

the eigenvector E^0 associated with the zero eigenvalue of the linearization of the map along the J_0 curve. Under these conditions, the image of W^u in the neighborhood of the intersection develops kink. For a slightly greater amount of unmodeled disturbance (a more-negative value of v), the kink opens into a self-intersecting loop of W^u (Fig. 15E). The remaining transitions (F and G) consist of a preimage of the self-intersection point moving from a point on W^u between the two intersections with J_0 (behavior E), to coincidence with one of the intersection points (behavior F and Fig. 14), and finally to outside the two intersection points (behavior G).

We see how the kink of behavior D forms by considering a *locally* $0/2$ preimage-behavior map of the plane $I = (y, z) \mapsto (f(y, z), g(y, z))$ in the neighborhood of a point (y_0, z_0) on a J_0 curve. This means the two eigenvalues of the linearization about (y_0, z_0) are 0 and some real a. We put the system into its normal form[4] and define a line L passing through the origin and parameterized by t:

$$L = \{(y, z) \in R^2 : y = \alpha t, z = t \quad \forall \quad t \in R\}. \tag{9}$$

[4] We shift (y_0, z_0) to the origin, and the system is rotated so that the eigenvector associated with the zero eigenvalue is parallel to the ordinate of the new coordinate system and the other eigenvector is parallel to the abscissa.

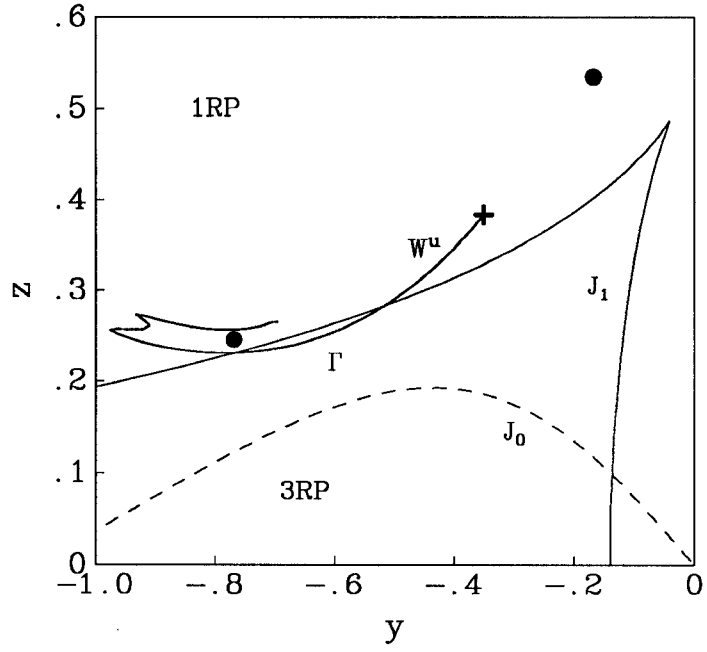

Figure 12 The H map for $v = -0.14$ with a portion of the saddle-unstable manifold (denoted Γ) just dipping into the 3RP region.

The image of L under a map consisting of the Taylor's series of I about (y_0, z_0) gives

$$\begin{aligned} y - f(y_0, z_0) &= a\alpha t + \left(f_{yy}\alpha^2 + 2f_{yz}\alpha + f_{zz}\right) t^2/2 + \mathcal{O}(t^3), \\ z - g(y_0, z_0) &= \left(g_{yy}\alpha^2 + 2g_{yz}\alpha + g_{zz}\right) t^2/2 + \mathcal{O}(t^3) \end{aligned} \tag{10}$$

so it is easy to see that when $\alpha = 0$ (when I corresponds to the zero-eigenvector), the right-hand-side of (10) is a function of t^2 and higher-order terms (provided *both* f_{zz} and g_{zz} do not vanish together), thus images of curves passing through (y_0, z_0) that are tangent to the zero-eigenvector at that point fold onto themselves as $t \to 0$.

Looking at the image (right-hand) side of Fig. 15A, we see W^u crossing J_1 in a manner reminiscent of the Γ segment of Fig. 12. This implies an additional loop of preimage on J_0 that maps to the W^u segment inside the 3RP region. This loop has its origins in the mechanism responsible for the $H^{-1}(\Gamma)$ loop of Fig. 13, but then proceeds through a sequence of transitions analogous to those of Figs. 15A through G, giving the figure-8 shaped loop of Fig. 16. Figure 16 corresponds to behavior 15F, the case where the self-intersection point touches J_1 and so has only two preimages. This is the reason for the coincidence of the figure-8 loop twist-point (one of the two preimages of the self-intersection point) and one intersection of W^u and J_0 in Fig. 16.

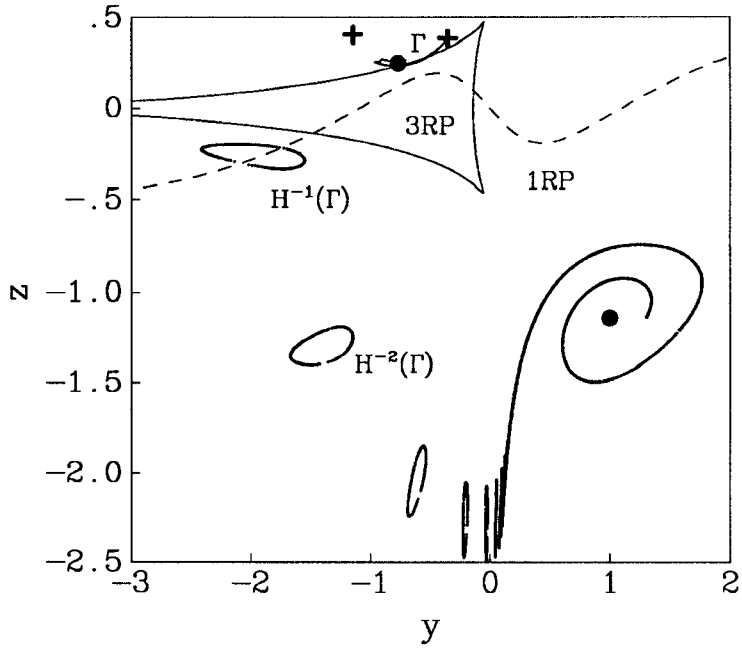

Figure 13 An expanded view of the previous Figure. The 30 "excess" preimages of Γ are the closed loops that asymptotically approach the set point $(y = 1, z = -1.14)$ in reverse-time.

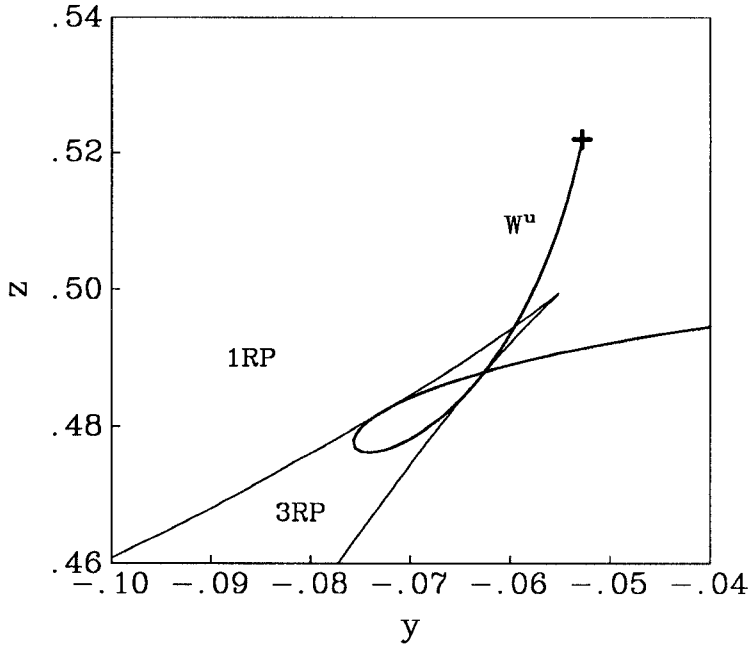

Figure 14 The H map for $v = -0.16$ demonstrating a self-intersecting saddle-unstablemanifold.

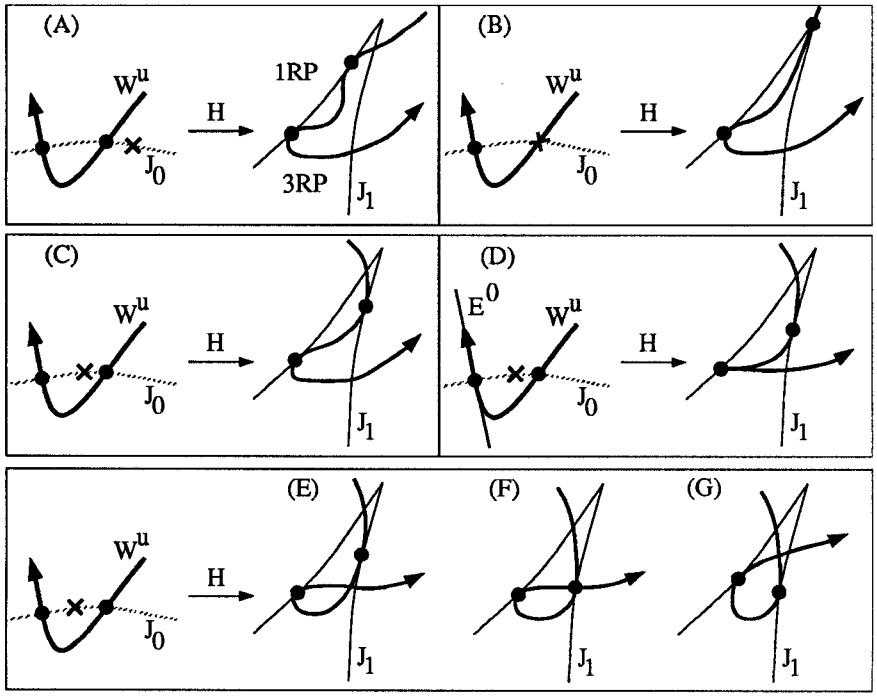

Figure 15 The transitions corresponding to decreasing v leading to the self-intersecting saddle-unstable manifold of the previous Figure. The "X" on J_0 marks the preimage of the cusp.

Concluding Remarks

This paper gives a sample of the global dynamical behavior displayed by noninvertible, discrete-time systems. These systems are characterized by nonunique preimage behavior that changes qualitatively with phase-space location. The systems discussed all arise from the adaptive control of linear, scalar plants with one unknown parameter that is estimated online. Thus, this work concentrates on dynamical phenomena displayed by noninvertible maps of the plane.

The importance of understanding the reverse-time dynamics of the closed loop systems becomes apparent in cases of multistability—situations where the locally-stable set-point coexists with another, undesirable attractor. Perturbations which drive the system from the set-point are quantified by computing the boundary of its basin of attraction. For the systems studied, these structures consist of the set of all preimages of local stable manifold segments associated with saddle-type periodic points. Called "stablemanifolds," they differ from the global stable manifolds of invertible systems (diffeomorphisms) in that they may not be manifolds: when basin boundary segments cross the *critical curves* separating regions of qualitatively-different preimage behavior, the preimages become disconnected and distorted, leading to complicated structures in phase space.

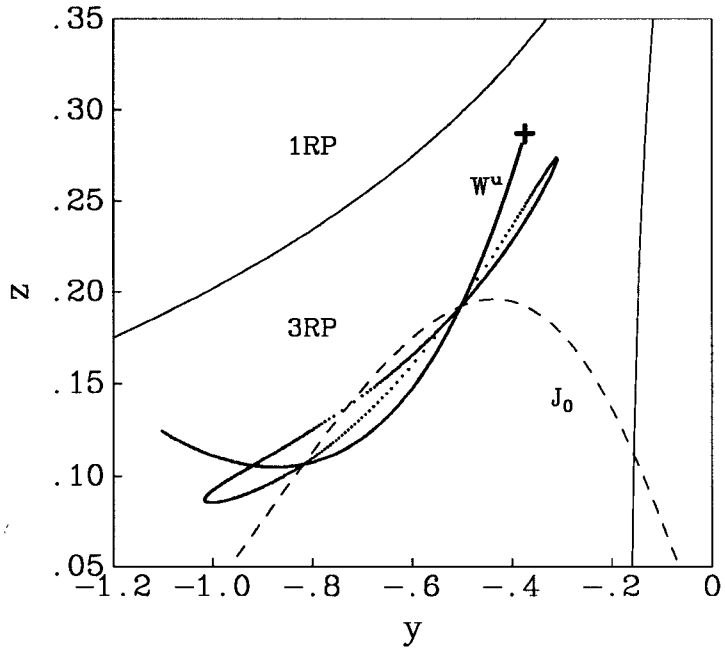

Figure 16 Preimages of the self-intersecting portion of the saddle-unstablemanifold showing the interaction with J_0 leading to self-intersection and the two additional preimages that glue to one another at J_0 giving a closed loop of preimages.

The complexity of basin structures is not always infinite, as one might first suspect from the geometrically-increasing reverse-time branching behavior of these systems. For example, a basin "island" (a disconnected portion of a basin of attraction) can be followed backward in time to find that all of its preimages originate in a region of phase space where the inverse-map has no real roots. However, if this basin island lies on a saddle-*unstablemanifold*, it will have at least one infinitely preiterable path in reverse-time. We thus see how complexity-level changes are associated with global (homo- and heteroclinic) bifurcations.

Having shown that basin structure complexity levels can change when basin boundaries cross unstablemanifolds, we see the incentive for studying the forward-time dynamics of noninvertible systems. As with stablemanifolds, the union of all images of local saddle-unstable manifolds can give rise to structures which are not manifolds: the global *unstablemanifolds* for noninvertible maps of the plane can develop kinks and self-crossings, behaviors not displayed by 2-dimensional invertible maps. We also find "excess" preimages of saddle-unstablemanifold segments due to preimage behavior changes in phase space, contributing additional features to the intricate and interesting global dynamical picture of these systems.

Acknowledgment

RAA acknowledges the support of the SRC through NSF grant ECD-8803012–06.

References

Adomaitis, R. A. and I. G. Kevrekidis (1990). On the global bifurcation characteristics of adaptive systems. *Proc. IFAC '90 11th World Congress on Autom. Cntrl.*, **4**, 299-304.

Adomaitis, R. A. and I. G. Kevrekidis (1991). Noninvertibility and the structure of basins of attraction in a model adaptive control system. *J. Nonlinear Sci.*, **1**, 95-105.

Adomaitis, R. A., I. G. Kevrekidis, and R. de la Llave (1991). Predicting the complexity of disconnected basins of attraction for a noninvertible dynamical system. *Systems Research Center Technical Report TR 91-41.*

Frouzakis, C. E., Adomaitis, R. A., and I. G. Kevrekidis (1991). Resonance phenomena in an adaptively-controlled system. *Int. J. Bifur. Chaos*, **1**, 83-106.

Frouzakis, C. E. (1991). The dynamics of an adaptive system with constant unmodeled disturbance. Manuscript in preparation.

Golden, M. P. and B. E. Ydstie (1988). Bifurcation in model reference adaptive control systems. *Systems & Control Letters*, **11**, 413-430.

Goodwin, G. C., Ramadge, P. J., and Caines, P. E. (1980). Discrete-time multivariable adaptive control. *IEEE Trans. Automat. Contr.*, **25**, 449-456.

Gumowski, I. and C. Mira (1980). *Recurrences and Discrete Dynamic Systems*, Lecture Notes in Mathematics #809, Springer-Verlag, Berlin.

Lorenz, E. N. (1989). Computational chaos—A prelude to computational instability. *Physica D*, **35**, 299-317.

Mareels, I. M. Y. and R. R. Bitmead (1986). Nonlinear dynamics in adaptive control: chaotic and periodic stabilization. *Automatica*, **22**, 641-655.

Mareels, I. M. Y. and R. R. Bitmead (1988). Nonlinear dynamics in adaptive control: chaotic and periodic stabilization-II. Analysis. *Automatica*, **24**, 485-497.